Experimental And Numerical Studies On Various Section Geometries For Inward Inversion

Ram Ranjan Sahu, Dr. Pramod Kumar Gupta

Abstract: -The inward inversion is one of the large deformations phenomenon in which the material deform inside the geometry. This phenomenon has been of great interest for its constant force displacement graph of deformation. The energy absorption through inward inversion can be of great use for devising the apparatus to absorb energy for impact or crash. The inward inversion to different shell section was planned to study force displacement graph in details. The energy absorption by different sections was compared. Analytical approach was adopted to simulate the experiment. The gained confidence in simulation was carry forward for generating more sections and for parametric study. The better shape of energy absorption could be suggested through this paper.

Keywords: - *Geometrical shell, Inward inversion, Large Deformations, Energy absorption, load-deflection, Finite Element analysis*

1. Introduction

Experimentally and analytically inward inversion of capped-end frusta as impact energy absorbers was studied by A.A.N. Aljawi et al [1]. The effect of parameters like frustum angle, wall thickness, and materials on inward inversion was studied. Finite element (FE) modeling and analysis of the deformation modes were also presented. They found that average load increases with increasing angle of frustum & wall thickness. For high values of height 'h' to thickness 't' ratio, specific energy of deformation is less than that for lower values of 'h/t'. Their study found good agreement between FE and experimental results. Experimental and theoretical studies were done on thin spherical shells under axial loads by N.K. Gupta et al [2]. Analytical simulations were carried out by ANSYS software. All deformation stages of the shell including non-symmetrical lobe formation were simulated. All nonlinearities i.e. material, geometric and contact were incorporated in the analysis. They discovered that relatively thick shells deform axi symmetrically and major load is absorbed by the rolling plastic hinges. When the thickness is reduced considerably, the inward dimpling is followed by non symmetric multiple number of lobes, which are caused by the formation of stationary hinges. Finite element analysis was done on tube inward curling process by conical dies by Yuung-Ming Huang [3]. They found that the tubes can be inward-curled for the die angle below the critical one of 123 degree. The diameter of inward-curling increased with increasing die angle. Smaller die angle had larger load as it was difficult for tube end to insert into die forming. A study on mode of collapse on frusta of varying wall thickness was done by P. K. Gupta [4]. The mode of collapse and energy absorption capacity was studied. All frusta deformed in axisymmetric mode due to development of associated plastic hinges. Mode of collapse was simulated using a nonlinear Finite Element code FORGE2. Contours of equivalent strain, equivalent strain rate, nodal velocity distribution, hoop stress and principal stress were extracted and interpreted them on collapse modes. The geometrical featured frusta were studied by R. R. sahu et al [5]. Feature changes were in shape, apical angle, steps, thickness etc. The parameters which could not be obtained physically were simulated analytically for parametric studies. The significance of features on inversion was studied experimentally and analytically. They found that the step kind of features facilitate the inversion. The wavy geometry creates ripples in force displacement graph. The frusta angle played important role and they found that the less the angle more will be the energy absorption. In their work they gave a guide line on parameters to be taken for good energy absorption, in inward inversion process. The collapse of thin-walled structure having symmetrical section can be concertina or diamond mode or a mixture of both, when subjected to axial loads. The collapse through inversion mode on these structures was reported by Al-Hassani et al. [6]. Various geometrical shell sections have potential to absorb energy while undergoing large deformation phenomenon. A Comparative analysis is planned on inversion phenomenon of thin walled structures with various section geometries.

- PhD scholar, Civil Engineering Department, IIT Roorkee, India (Working as Assistant General Manager in Engineering Research Centre of TATA Motors-Pune, through Tata Technologies, Pune, India) Correspondence: A1-404, Kumar Prerana, Aundh, Pune (MH), Pin 411007 India
  Email: RamRanjan.Sahu@tatatechnologies.com
  Cell Phone No: +91 9881461360
- Associate Professor, Correspondence: Structural Engineering Department of Civil Engineering, IIT Roorkee, (Uttarakhand), Pin 247667 India
  Email: pkgupfce@iitr.ernet.in,
  Cell Phone No: +91 9411500841

2. Experiments

2.1 Experimental setup

The experimental setup has three main components i.e. samples for testing, fixture to hold and apply load and the machine for load application. The samples are hand made from capped end circular cylindrical shape which is made through spinning process. Example is shown for square and hexagonal shape, as shown in Figure 1a. The average perimeter was kept 467mm and thickness to 1.5 mm for all shapes. Few samples photographs of test samples are shown in Figure 1b.

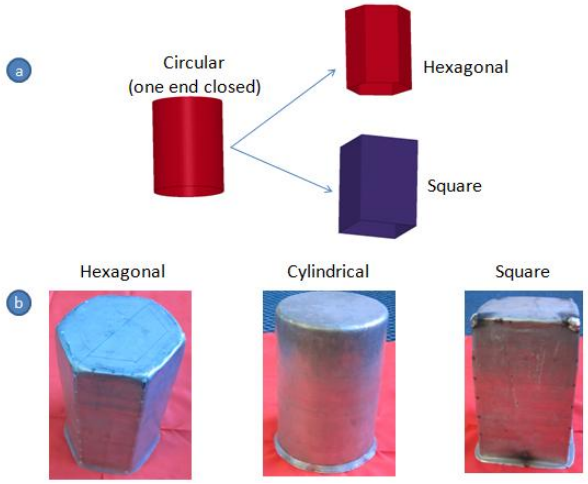

Figure 1: Test samples

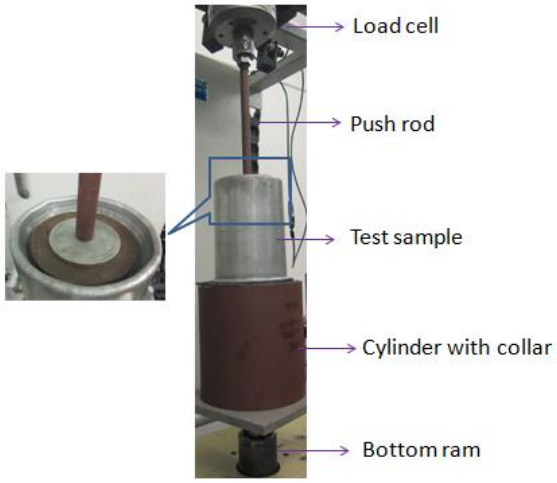

Figure 3: Test setup

Special fixtures are required for inversion process. Few photographs are shown in Figure 2. It has washer of 8mm thickness made of steel (Figure 2a), which is kept in pair to the capped end of sample. One washer is kept at the top and one below the cap. Then the push rod (Figure 2d) threaded end is inserted through the hole of washers and sample. A nut is used to tight with the thread. Hence the capped end acted monolithically with washer whiles applying load. Bottom support plates (Figure 2b) are of the shape of samples. These plates facilitate the inversion process below the bottom level of samples. This is kept above the cylinder. The cylinder (Figure 2c) has a collar on which the support plate is kept. Samples are kept above bottom support plate.

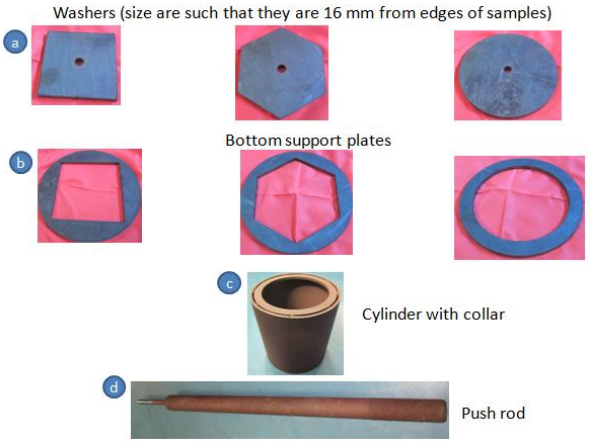

Figure 2: Test Fixtures

The load is applied by giving enforced motion through Instron universal testing machine. The machine has maximum capacity up to 4 ton. The load cell is kept below the top stud. The push rod is fixed to the load cell. The bottom sides ram moves up and down with maximum ram stroke up to +/- 125 mm. The system is hydraulically operated and can operate at quasi static and at transient load conditions. The ram on which cylinder is kept, was moved up with speed of 10mm/min to ensure the quasi static condition. The alignment of test samples and its fixture is assured with machine axis. The testing was done to maximum displacement up to 200mm. The test setup is shown in Figure 3.

2.2 Material properties

The material tensile was performed with the material testing samples which were prepared as per the specifications ASTM E8 [7] as shown in Figure 4.

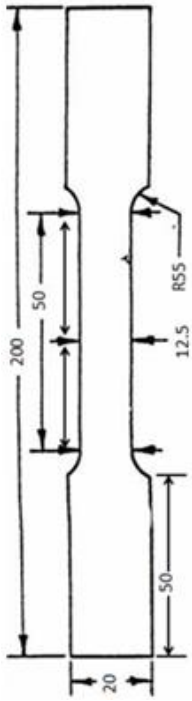

Figure 4: Material test sample specifications

The test was repeated with many samples. From the test graph, the material tensile strength extracted as per ASTM E 8 was 108MPa@4.6% strain and yield strength=65MPa. The fixtures were made of steel and they are quite thick and hence were treated as rigid.

2.3 Experimental results

The deformation pattern of three samples picture are shown in Figure 5. Left to right pictures are in deformation progress order. It is observed that the circular shape has smooth inversion process as shown in Figure 5a. For hexagonal and square shapes (Figure 5b-c) the perimeter is reshaped on more load application. The new lobes are generated and the

shapes get changed. The experiment had aim to start and establish the inversion process. Once the instability like local buckling or tearing was noticed, experiment was stopped. The data handled were for the established process only.

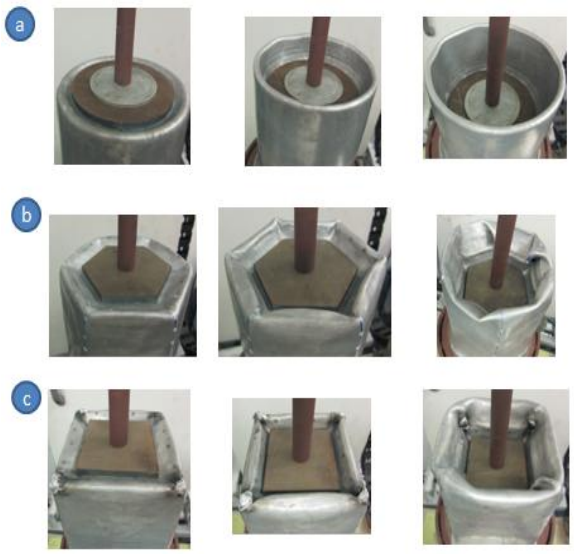

Figure 5: Deformation pattern of samples

Their respective force deformation graph is shown in Figure 6. The circular (Figure 6a) and hexagonal shapes (Figure 6b) have smooth start. The square shape has turbulence in force displacement graph as marked in Figure 6c. It can be attributed to reshaping through new lobe formation.

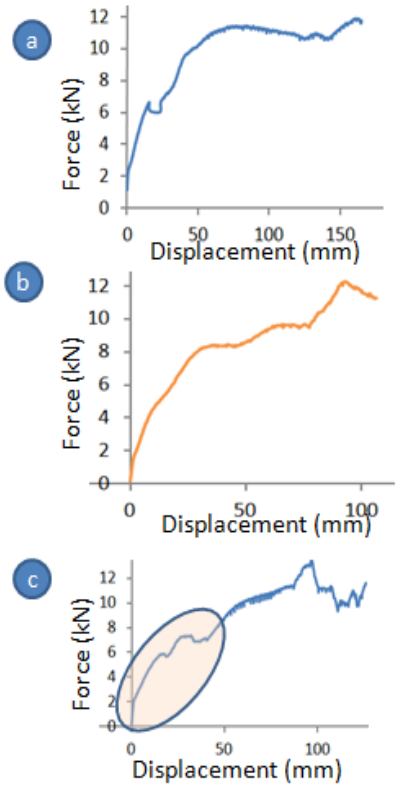

Figure 6: Force-Displacement Graph

3. Numerical simulation

Finite element (FE) is a numerical tool to apply for various experimental simulations, analyze the behavior of engineering structures in variety of conditions. Many researchers have been customizing this tool and developing various elements for specific purposes. Venkat Aitharaju et al. [8] had developed zigzag elements for composites and applied those elements for crash analysis of automotive fibers. Ramtekkar et al. [9] have used mixed FE modeling approach for analysis of laminated fibers and for their vibrations analysis. Finite element (FE) simulations were carried out for tested samples and correlated to test results. Once the confidence to correlation was established, the other section could be FE modeled, solved and result could be studied. The different stages of FE simulation are as follows:

3.1 FE Model Building through HyperMesh

The Altair product HyperMesh [10] is used for FE model building. Samples are presented with 4 node shell elements at mid geometry surface. The bottom fixture is modeled shell elements with rigid material property. It is given an upward enforced motion of 200mm. The top fixture is also modeled with rigid material and is fixed in place. FE model generated through HyperMesh gave good convergence and good correlation to test data.

3.2 Problem solving through LsDyna

LsDyna [11] explicit FE solver is used for solving the problem. LsDyna has lot of material models to define the sample and fixture materials. Also it offer lot of contact algorithm to define the contacts occurring during experiment. LS-Dyna uses the explicit central difference scheme to integrate the equation of motion wich is derived from the below force balance constitutive equation

$$F_I + F_{D+} F_{int} = P(t) \quad (1)$$

Where F_I=Inertia force

F_D=Damping force

$F_{int=}$ Internal forces

The closed form solution to above equation is as below

$$u(t)=u0\cos\omega t+\dot{u}/\omega\sin\omega t+(p0/k)*1/(1-\beta^2)*(\sin\varpi t-\beta\sin\omega t) \quad (2)$$

where

u0 = Initial displacement

$\dot{u}$ = Initial velocity

p0/k= Static displacemnt

ω = circular frequency

β= Load frequency

The centre difference method can be described with below semi-discrete equation of motion, at time n is

$$Ma^n = P^n – F^n + H^n \quad (3)$$

Where M is the diagonal mass matrix, P^n accounts for external and body force, F^n is the stress divergence vector and H^n is the hourglass resistance. To advance to time t^{n+1}, central time diffrence is used

$$a^n = M^{-1}(P^n – F^n + H^n)$$

$$v^{n+1/2} = v^{n-1/2} + a^n \Delta t^n$$

$$u^{n+1} = u^n + v^{n+1/2} \Delta t^{n+1/2}$$

where

$$\Delta t^{n+1/2} = (\Delta t^n + \Delta t^{n+1}) /2$$

v and u are the global nodal velocity and displacemnt vectors, respectively. Geometry is updated by adding the displacemnt increments to the initial geometry

$$X^{n+1} = x^0 + u^{n+1}$$

Though this method requires more storage for displacement vector, the results are less sensitive to round-off error.

3.2.1 Material Modeling

The fixtures are modeled with rigid material which can be defined by *mat_rigid which is material 20. An elastic-plastic sample material with stress versus strain curve obtained from the test could be defined by *mat_piecewise_linear_plasticity. This is Material Type 24.

3.2.2 Contact Modeling

The contact between fixtures and samples were defined by *contact_automatic_surface_to_surface. Test samples were given *contact_automatic_single_surface_id for self contact. The automatic contact options are opted as these contacts are non-oriented and they can detect penetration coming from either side of a shell element. Coulomb friction [12] type was used to define the coefficient of friction between contacts.

3.3 Result interpretation

The solved problems were post processed with LS-PrePost for result interpretation. This is an advanced interactive program for handling varieties of result data. Figure 7 shows the FE shell model for the hexagonal sample. This model fully represents the geometry of the sample and experimental arrangement. Shell element formulation proposed by Belytschko-Tsay [13] was used. In this formulation the shell geometry is assumed to be perfectly flat, the local coordination system originates at the 1st node of the connectivity, and the co-rotational stress update does not use the costly Jaumann stress rotation [14]. Results generated with this shell element usaually compare favorably with those of more costly shell elenents.

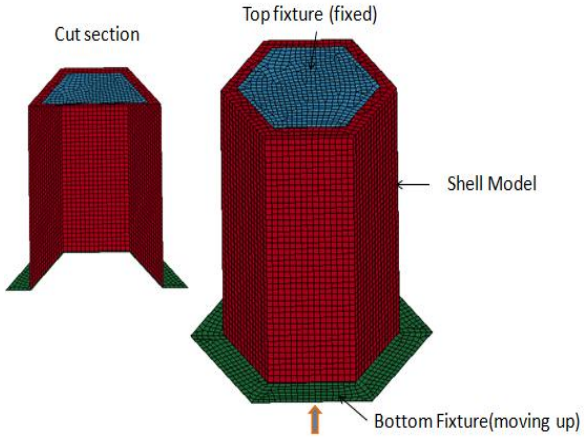

Figure 7: FE Model for hexagonal section geometry

Good energy balance ensures correctness of simulation. Figure 8 shows the energy balance graph of simulation of circular section. From the graph it is evident that the unwanted energy like kinetic, hourglass, sliding etc is minimum and the internal energy is solely generated due to shell deformation.

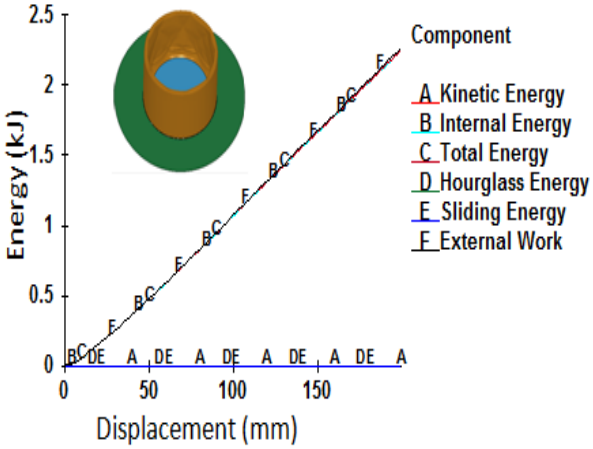

Figure 8: Energy balance graph for circular section

Also the FE deformed cut section and actual sample cut section for circular section is shown in Figure 9. The shapes matched well. It revealed that the material test data taken into analytical analysis, contact algorithm used, element type and their formulation choose worked well.

Figure 9: Cut section for circular section

4. Result & discussion

A typical FE simulated graph of hexagonal section is shown in figure 10, to explain the force displacement characteristics. The force displacement graph start with increasing quasi static force to a maximum value as marked by zone 1. This is the force required to generate plastic hinge at the capped end. Once plastic zones are created, the incubation takes place as marked by zone 2. In this zone force reduces and the incubation further facilitates the inversion process. On further load application, the lobes formation at the corner starts which is marked by zone 3. Due to lobes formation, the force value increases. In zone 4, it is shown that the reshaping takes place in periphery. Complete new cross section can be noticed in this zone.

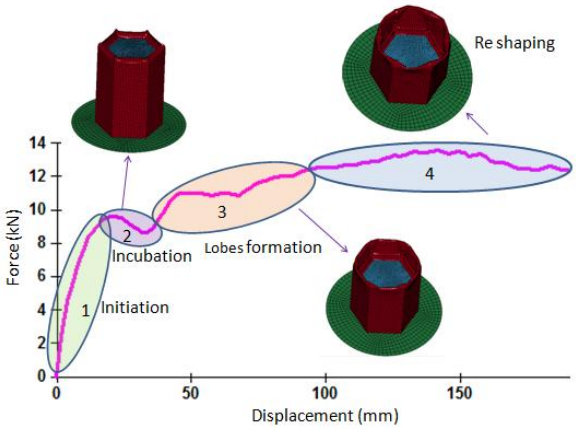

Figure 10: Typical force displacement graph

The experimental and theoretical force displacement graph are superimposed and plotted in Figure 11. They matched to agreeable limit. The variation could be attributed in thickness variation on sample which is made with spinning process where a constant thickness throughout the height cannot be assured. Another factor could be software limits, like it assumes yield value at zero strain and that is why an initial peak is noticed in theoretical graph.

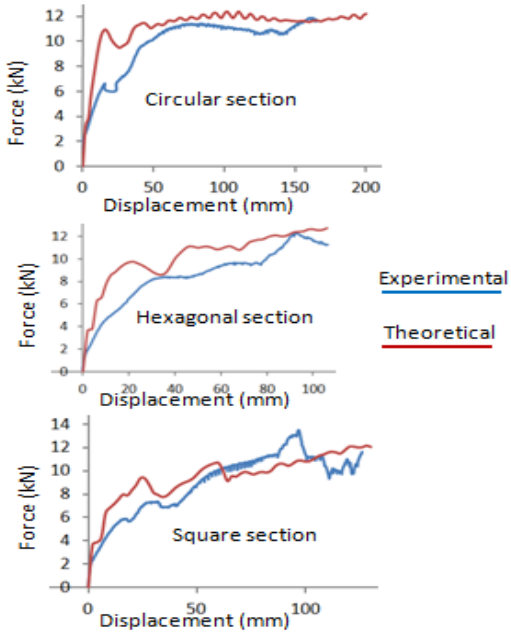

Figure 11: Experimental and theoretical graph comparison

The force displacement graph for triangular and circular section is shown in Figure 12. From the graph it can be observed that the force displacement graph for triangular section is quite wavy from start to finish while it can be said sooth for circular section. The more the numbers of edges in the section more smooth is the graph while for fewer numbers of edges, it is vice versa. The shape which had fewer numbers of edges reshapes to a section of higher numbers of edges, to facilitate the inversion process. For sections with more numbers of edges, do not require much effort since they have more numbers of edges which assist in inversion process.

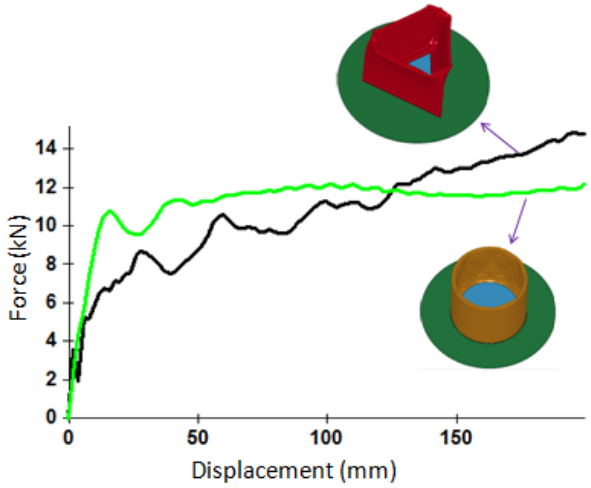

Figure 12: Force displacement graph comparison for triangular and circular section

The sections studied theoretically for inversion, are enlisted in Table 1 with their specific energy. Also the bottom fixture up stroke '(H)', the maximum force 'F (max)' at the end of displacement and average force 'F (avg)' is also mentioned in the table.

Table 1: Energy and forces of different sections

Sample	Stro--ke (H) mm	Invers-ion length (H/2)	Ene-rgy (kJ)	Deflec-ted portion wt (kg)	Sp ener-gy (kJ/kg)	F(av-g) =(kJ)/H	F(max) (kN)
Tria	200	100	2.14	0.23	9.30	10.7	14.9
square	200	100	2.18	0.243	8.97	10.9	14.5
Rectangle	200	100	2.17	0.237	9.16	10.9	13.3
Hexagonal	200	100	2.3	0.252	9.13	11.5	12.5
Frusta	200	100	1.73	0.206	8.40	8.7	9.6
Pyramid	200	100	2.19	0.232	9.44	11.0	13.1
Circular	200	100	2.24	0.258	8.68	11.2	12.2

The specific energy capacity (kJ/kg) of various sections is compared in the Figure 13. Frusta and circular that have infinite numbers of edges shows least energy absorption capacity in inversion process while pyramid, triangular etc who have finite numbers of edges absorbed more energy in the process.

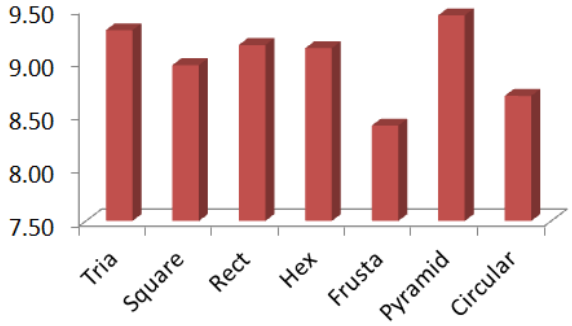

Figure 13: Specific energy comparison

The difference in maximum force extracted at the end of displacement and average force is shown in Figure 14 for the process. The least difference was found for the circular and frusta section. This can be attributed to their uniform force displacement graph.

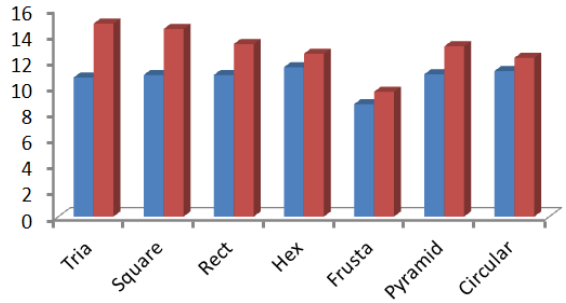

Figure 14: Maximum and average force comparison for different section

Figure 15 shows the deflected shapes for triangular, square, rectangular and hexagonal cross sections while Figure 16 shows deflected shapes for frusta, pyramid and circular section. These deflected shapes are at initial and at the end of the inversion process along with their force displacement graph. The inversion process tends to reshape the sections into the shape with more numbers of edges which could facilitate the inversion process. In doing so, the section with fewer numbers of edges required more force for reshaping, for example triangular and square sections. Their graph is also rough which is attributed to reshaping and its force requirement.

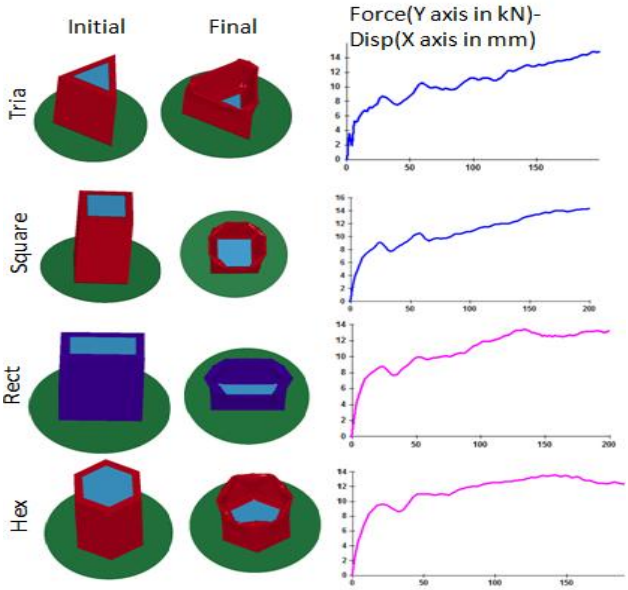

Figure 15: Deflected shapes of triangular, square, rectangular and hexagonal section with their force displacement graph

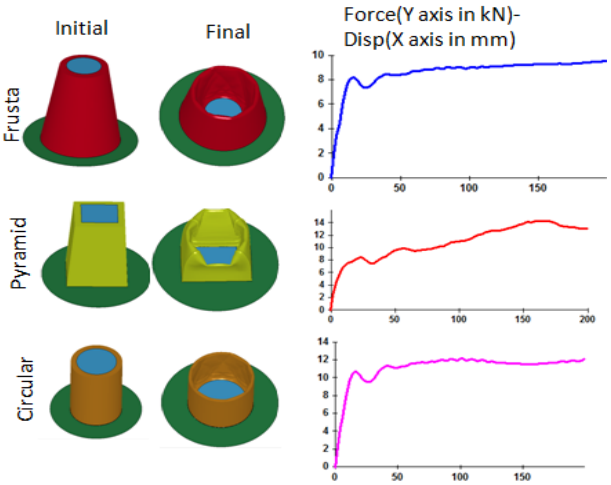

Figure 16: Deflected shapes of frusta, pyramid and circular section with their force displacement graph

The element behavior in terms of stress variation in vicinity to top edges for circular and triangular section is shown in Figure 17 a-b. For the circular section the variation is less (Figure 17a), as the inversion process is smooth to this section. For triangular section, the element (S991) at the middle of the edge, stress behavior is different than to the elements at the corners (S654, S1095) as shown in Figure 17b. The corner element are subjected to more stress variation due to the process of reshaping, while it is less for the mid edge element.

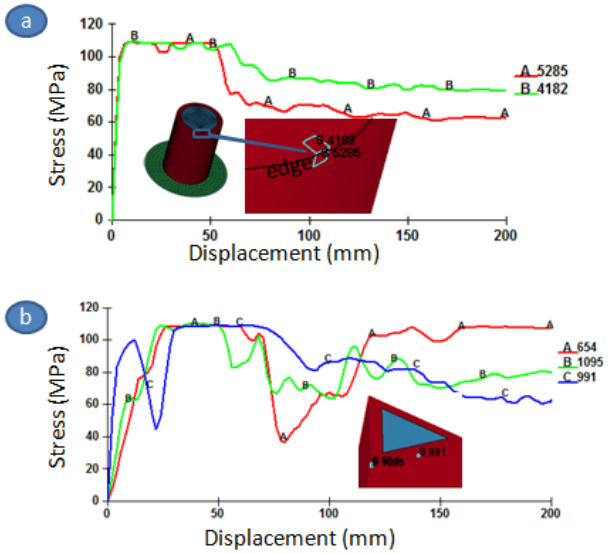

Figure 17: Stress variation of corner and edge elements

The superimposed force displacement graph for all sections is shown in Figure 18. From the graph it is evident that the more turbulence in graph is noticed for the section having less numbers of edges for example triangular and four edged sections (square, rectangular, pyramid). Their maximum force at the end of displacement is also higher. The least force is noticed for the frusta and maximum for the triangular section at the end of displacement.

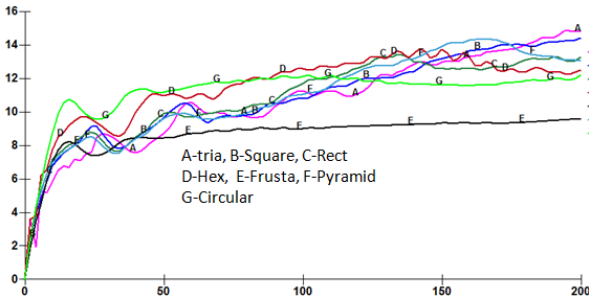

Figure 18: Superimposed force displacement graphs of all sections

The thickness of circular section was increased and force displacement graph plotted along with test result as shown in Figure 19. The force required for higher thickness is more for obvious reason. This phenomenon can be harnessed for higher energy absorption requirement. The experimental graph lies between thickness of 1.4mm and 1.5mm. Small thickness variation is expected to the samples for experiment, since they are made from spinning process and their thickness lies between these two thicknesses.

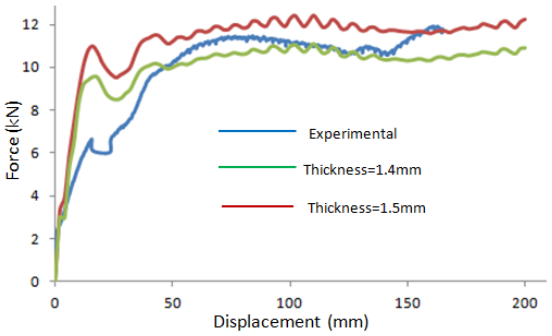

Figure 19: Thickness change effect on circular section

5. Conclusion

The inversion process for different sections is discussed in details. The FE analysis adapted for parametric and to studies the more sections which were not possible to make in real sense. The experiment showed that the reshaping towards a circular section takes place for sections having fewer numbers of edges. In doing so they require more force and hence they absorb energy. Also it is noticed that the force displacement graph of sections having less numbers of edges have turbulence while the circular or frusta section have smooth graph as they have infinite edges in section which assist in smooth inversion process. The average and maximum force difference is less for circular and frusta section which is prerequisite for good energy absorber. Though the sections with less numbers of edges may show great energy absorption capacity in inward inversion, they can be judicially used in devising energy absorption device.

ACKNOWLEDGEMENTS

The authors gratefully acknowledge experimental support provided by engineering research centre of TATA Motors, Pune-India. Also thanks its proto shop for workman ship provided to build the complex model from a circular section.

REFERENCES

[1]. A.A.N. Aljawi, A.A.A. Alghamdi, T.M.N. Abu-Mansour and M. Akyurt, “Inward inversion of capped-end frusta as impact energy absorbers”, Thin-Walled Structures, 43:647–664, (2005)

[2]. N.K. Gupta, N. Mohamed Sheriff and R. Velmurugan, “Experimental and theoretical studies on buckling of thin spherical shells under axial loads”, International Journal of Mechanical Sciences, 50: 422–432, (2008)

[3]. Yuung-Ming Huang, “Finite element analysis of tube inward curling process by conical dies”, Journal of Materials Processing Technology, 170:616–623, (2005)

[4]. P.K. Gupta, “A study on mode of collapse of varying wall thickness metallic frusta subjected to axial compression”, Thin-Walled Structures, 46:561–571, (2008)

[5]. Ram Ranjan Sahu, Pramod Kumar Gupta, “ Studies on geometrical featured metallic shell structures for inward inversion”, International journal of civil engineering and technology (ijciet), 3:251-264, (2012)

[6]. Al-Hassani STS, Johnson W, Lowe WT, "Characteristics of inversion tubes under axial loading", J Mech Eng Sci, 14:370–81(1972).

[7]. ASTM International ASTM E8 / E8M - 09 Standard Test Methods for Tension Testing of Metallic Materials.

[8]. Aitharaju VR, Averill RC, "C-0 zig-zag finite element for analysis of laminated composite beams", Journal of engineering mechanics-ASCE, 125(3) 1999.

[9]. Ramtekkar G. S, Desai Y.M, Shah A. H, "Mixed finite element model for thick composite laminated plates", Mechanics of Adv. Material & Structures 9(2):133-156(2002).

[10]. HyperMesh11, A product of Altair Engineering HyperWorks.

[11]. LsDyna keyword user's manual. Volume 1 Version 960, Livermore Software Technology Corporation, pp251-261(chapter- contact).

[12]. LsDyna theory manual, Chapter 6, compiled by John O. Hallquist. Livermore Software Technology Corporation, 2876 Waverly Way, Livermore, California 94550-1740. May 1998.

[13]. LsDyna theoretical manual, May1998, Chapter 15. Livermore Software Technology Corporation, Livermore, California 94550-1740.

[14]. LS Prepost. Version 2.1, May 2007. Livermore Software Technology Corporation, Livermore, California 94550-1740.